Mid-Pleistocene links between Asian dust, Tibetan glaciers, and Pacific iron fertilization

Jinbo Zan[a,b,1] (ID), Barbara A. Maher[c,1] (ID), Toshitsugu Yamazaki[d] (ID), Xiaomin Fang[a,b] (ID), Wenxia Han[e] (ID), Jian Kang[a,b], and Zhe Hu[a,b]

Increasing Asian dust fluxes, associated with late Cenozoic cooling and intensified glaciations, are conventionally thought to drive iron fertilization of phytoplankton productivity in the North Pacific, contributing to ocean carbon storage and drawdown of atmospheric CO_2. During the early Pleistocene glaciations, however, productivity remained low despite higher Asian dust fluxes, only displaying glacial stage increases after the mid-Pleistocene climate transition (~800 ka B.P.). We solve this paradox by analyzing an Asian dust sequence, spanning the last 3.6 My, from the Tarim Basin, identifying a major switch in the iron composition of the dust at ~800 ka, associated with expansion of Tibetan glaciers and enhanced production of freshly ground rock minerals. This compositional shift in the Asian dust was recorded synchronously in the downwind, deep sea sediments of the central North Pacific. The switch from desert dust, containing stable, highly oxidized iron, to glacial dust, richer in reactive reduced iron, coincided with increased populations of silica-producing phytoplankton in the equatorial North Pacific and increased primary productivity in more northerly locations, such as the South China Sea. We calculate that potentially bioavailable Fe^{2+} flux to the North Pacific was more than doubled after the switch to glacially- sourced dust. These findings indicate a positive feedback between Tibetan glaciations, glaciogenic production of dust with enhanced iron bioavailability, and changes in North Pacific iron fertilization. Notably, this strengthened link between climate and eolian dust coincided with the mid-Pleistocene transition to increased storage of C in the glacial North Pacific and more intense northern hemisphere glaciations.

Asian dust | iron fertilization | Pacific productivity | biological pump | increased C storage

The biological productivity of substantial areas of the world's oceans, including the Southern Ocean and North Pacific, is limited by iron deficiency, which can be alleviated by the eolian transport and deposition of iron-bearing mineral aerosols (hereafter, "dust"). Supply of iron-bearing dust is thus both controlled by climate (amplified, for example, during cold, dry glaciations) and in turn affects the climate (1, 2). Iron fertilization by dust enhances ocean productivity, leading to enhanced take-up of dissolved carbon in seawater, subsequent drawdown of CO_2 from the atmosphere, and lowering of surface temperatures. As much as 50% of the decline in atmospheric CO_2 during past glaciations has been attributed to iron fertilization by eolian dust (3).

Mineral dusts derived from the vast arid regions of the Asian interior constitute the major source of iron for the North Pacific (4–7), an iron-limited high-nutrient, low-chlorophyll ocean region (8, 9). Away from the island arcs, Asian dust constitutes the dominant lithogenic component in the Pacific deep sea sediments, over an immense areal span encompassing the sub-Arctic, northwestern and tropical western Pacific (4, 10).

It has long been thought that increasing fluxes of Fe-bearing Asian dust, resulting from late Cenozoic global cooling, have exerted substantial impact on phytoplankton productivity in the North Pacific and thereby affected the global carbon cycle (2, 9, 11). Indeed, modern observational studies show that springtime dust transport events over the western North Pacific can increase ocean primary productivity by >70%, compared with non-dusty conditions (12). On glacial/deglacial timescales, modeling studies estimate that the North Pacific region contributed ~30% of the total (global) drawdown of atmospheric CO_2 during the last glaciation (3). Such studies thus indicate a significant role for Asian dust fluxes in driving ocean primary productivity, influencing the strength of the biological pump, and hence contributing to atmospheric CO_2 and surface temperature changes on a global scale.

Paradoxically, growing evidence suggests that North Pacific productivity maintained relatively low and constant values during the early Pleistocene glaciations, despite their higher associated dust fluxes (13–15). It appears that glacial stage increases in primary productivity and/or shifts in phytoplankton communities in the N. Pacific only occurred after the mid-Pleistocene transition (MPT) (14–16). These apparently contradictory

Significance

The amount of dust blown from Asian deserts is thought to fertilize iron-deficient areas of the North Pacific Ocean, increasing productivity and subsequent drawdown of atmospheric CO_2. But Pacific productivity remained low in early Pleistocene glaciations, when dust fluxes increased; only showing glacial upturns after the mid-Pleistocene (~800 ka ago). Solving this paradox, we show that the iron mineral composition of the Asian dust switched dramatically at ~800 ka, when Tibetan glaciers expanded, providing fresh, more reactive dust to the Pacific phytoplankton. The bioavailable iron supply doubled after this switch to glacial dust, correlating with increased productivity and/or phytoplankton community changes. This strengthened climate/eolian dust link coincided with increased C storage in the glacial Pacific and intensified northern hemisphere glaciations.

observations have sparked controversy regarding the impacts of Asian dust supplies on Pacific biogeochemistry and hence, on the global carbon cycle.

Here, we solve this paradox by identifying the evolution of the iron mineralogy of Asian dust, over a timespan of the last 3.6 My. Common to the majority of Pacific dust/climate studies is their focus on the *fluxes* (i.e., the mass of dust deposited/unit area/year; $g/m^2/yr$) of Asian dust, rather than its composition and likely bioavailability. Yet recent work has shown increasingly that particulate Fe^{2+} content, rather than total Fe concentrations, can control the Fe bioavailability of natural dusts (11, 17–21). Fresh, unweathered detritus derived from intense glacial erosion and/or tectonic activities is enriched in primary Fe^{2+}-bearing minerals, in sharp contrast to non-glaciogenic, desert sediments. The latter mainly contain stable, oxidized, Fe^{3+}-bearing minerals, due to long-term surface exposure and chemical weathering (11, 18–20). In the Asian dust source regions, intensive tectonic deformation and/or remarkable cooling since the late Cenozoic have resulted in substantial physical weathering and erosion of bedrock, especially in the Tibetan Plateau (22–24), producing immense volumes of primary Fe^{2+}-bearing minerals.

We analyzed the iron oxide and total iron content of the Asian dust recorded in a recently discovered terrestrial Asian dust sequence, on the northern slopes of the West Kunlun Mountains to the south of the Tarim Basin (TB)'s Taklimakan Desert (Fig. 1). Meteorological and geochemical evidence demonstrates that the fresh detritus eroded from the surrounding mountains of the northern Tibetan Plateau, and deposited in the deserts of the extensive ($\sim$560,000 km^2) TB, provides a major source of downwind sediment supply for Asian desert dust, the famous Chinese Loess Plateau (CLP) and the North Pacific (4–7). A 671 m-deep sediment core was recovered from a broad flat TB surface; multiple dating approaches show that this accumulated dust (loess) sequence accumulated from $\sim$3.6 Ma to the present (*SI Appendix, Supplementary Text*) (25). The climate in this intracontinental area, strongly influenced by the westerlies, is extremely arid (mean annual precipitation between $\sim$10 and 80 mm). Due to the minimal post-depositional weathering, paleosols are very weakly developed in the TB loess sequence. Here, detailed rock magnetic measurements of bulk TB loess samples were first performed, at 20 to 40-cm intervals (i.e., $\sim$1 to 3 ka in resolution). Then, the <5 μm fractions of the TB loess, representing the dominant eolian dust component transported to the North Pacific, were separated for further rock magnetic, geochemical, mineralogical, and diffuse reflectance spectroscopy (DRS) analyses, in order to investigate any temporal variations in their Fe oxide mineralogy, concentrations, and speciation (oxidation state).

Results

Our measured rock magnetic parameters, including mass-specific magnetic susceptibility (χ) and its frequency dependence (χ_{fd}%), saturation magnetization (Ms), and isothermal remanent magnetization (IRM), are sensitive to variations in the mineralogy, concentration and grain size of iron oxides in sediments (29–32). From 3.6 to 0.8 Ma, the magnetic concentration-dependent parameters of χ, IRM_{1T} and Ms of the TB bulk dust samples maintained relatively low values. After $\sim$0.8 Ma, they displayed dramatic increases (Fig. 2 A–C). The size-fractionated samples exhibit similar temporal variations in χ and IRM_{1T} as the bulk samples (Fig. 2 D and E). The bulk TB samples generally show slightly higher values of χ and IRM_{1T} than their <5 μm components (Fig. 2 A–E), and no frequency-dependence of χ at low
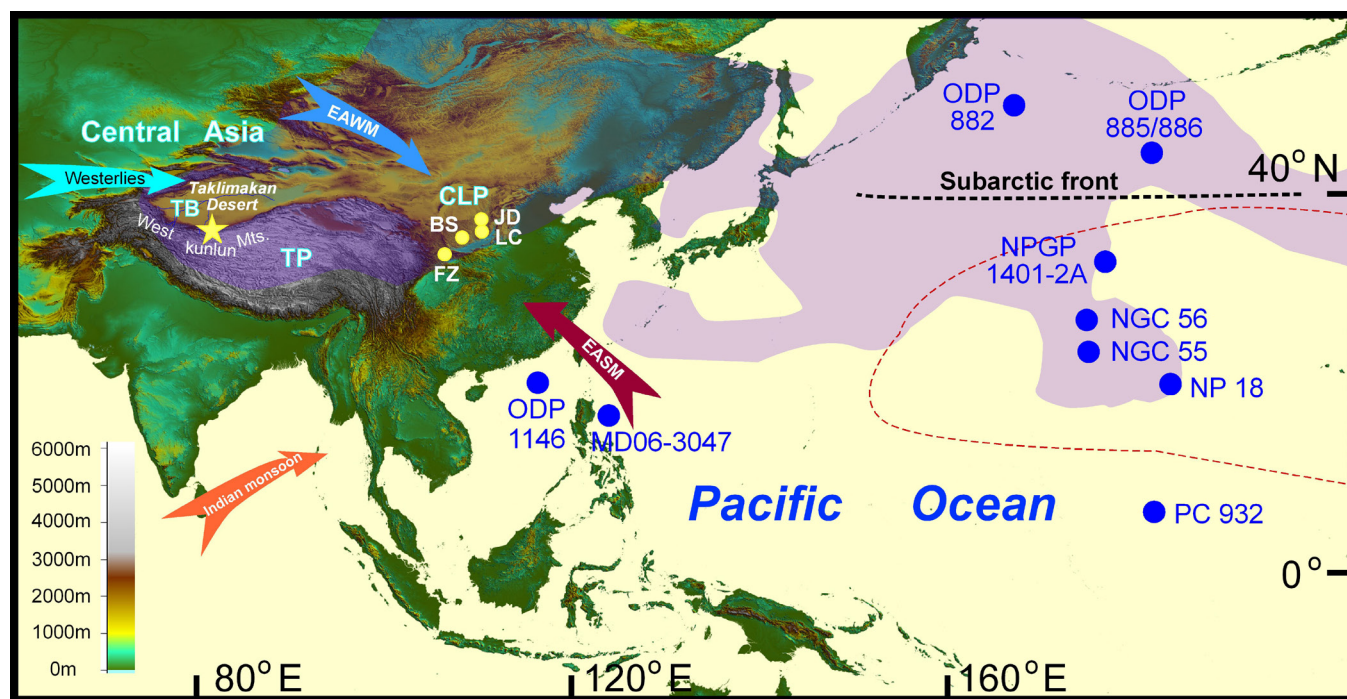

Fig. 1. Locations of the eolian dust profiles and pelagic sediment cores in the N. Pacific referenced in the text. The yellow star shows the location of the TB loess borehole. JD (Jiaodao), LC (Luochuan), BS (Baishui), and FZ (Fengzhou) represent loess profiles in the CLP. Arrows indicate the trajectories of Asian monsoon winds and westerlies; EAWM and EASM represent the East Asian winter and summer monsoons, respectively. The shaded area indicates the dust distribution arising from an extensive dust storm (7) which occurred in the Taklimakan Desert on May 8 to 9, 2007. The red dashed line indicates the central N. Pacific province where the lithogenic materials of pelagic sediments have similar Nd isotopic compositions to the Asian dust (26). Note that the NGC55 core is located at the center of these overlapping zones, suggesting that the TB dust supplies the dominant contribution to the silicate fraction of the central N. Pacific pelagic sediments. In contrast, the geochemical and mineralogical compositions of pelagic sediments in the sub-Arctic Pacific are influenced by diverse processes, including iceberg rafting, volcanic ash and/or deep-water upwelling (27), (28).
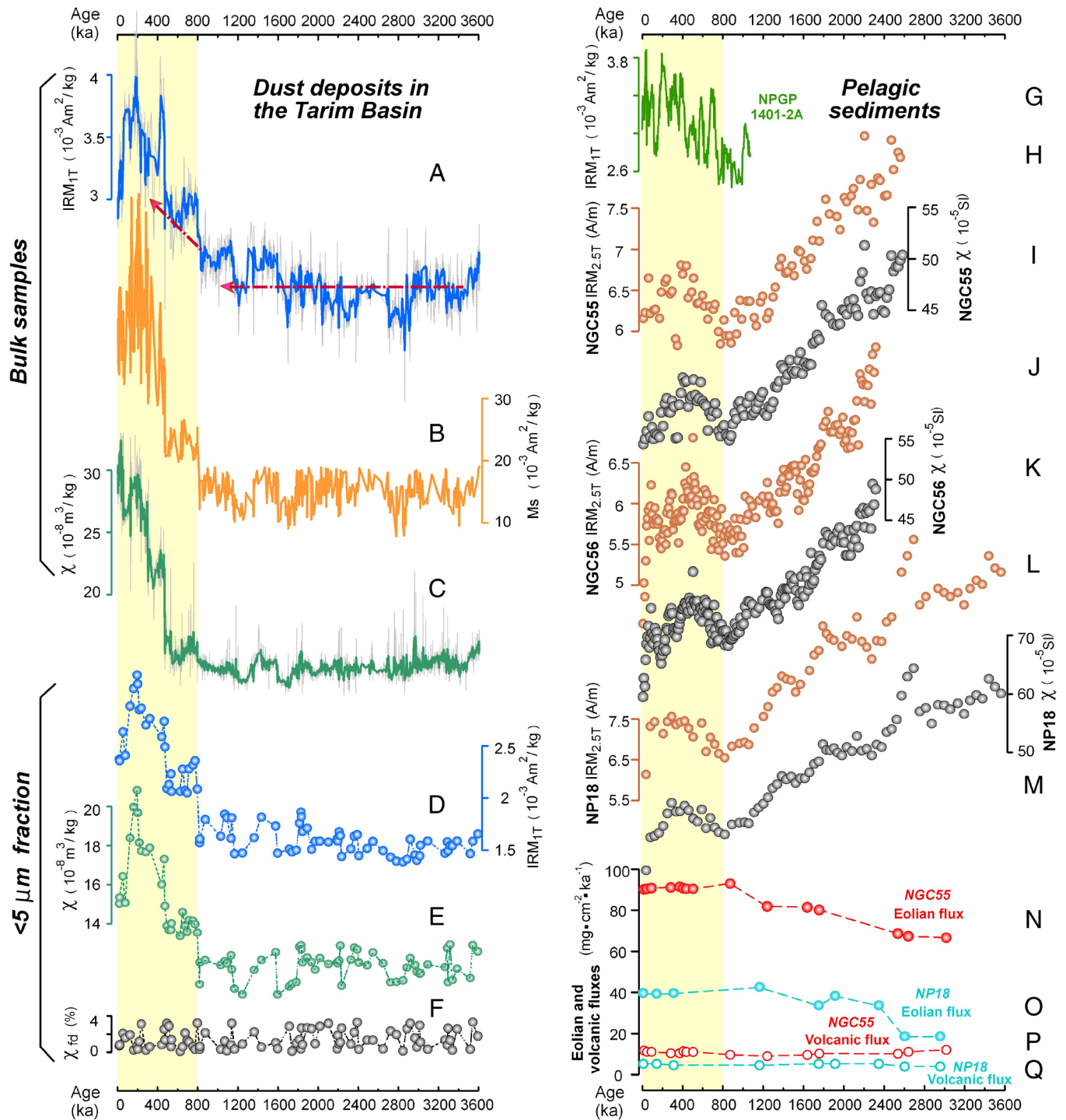
Fig. 2. Temporal variations in rock magnetic parameters of (*A–F*) bulk samples and the <5 μm fraction of dust deposits from the TB and (*G–Q*) pelagic sediments from the central N. Pacific (31, 33, 34). Note that the increases in ferrimagnetic content of the marine and terrestrial sediments occurred synchronously, around the MPT, indicating that the composition of allochthonous, eolian iron oxides deposited in the central North Pacific altered significantly at this time.

temperature is observed in the <5 μm TB fractions (Fig. 2*F* and *SI Appendix,* Fig. S1). All of these observations indicate that any post-depositional alteration of primary Fe-bearing minerals in the TB dust, induced by chemical weathering and soil formation, has been negligible from the Pliocene through to the present day.

Thermomagnetic analyses indicate that the magnetic behavior of the TB dust was dominated by hematite (Fe^{3+}-bearing) prior to the MPT but became dominated by magnetite (mixed Fe^{2+}/Fe^{3+}-bearing) after the MPT (*SI Appendix,* Fig. S2). This mineralogical shift is independently attested by the DRS measurements, which show that

concentrations of hematite and goethite (Fe^{3+}-bearing) maintained relatively high values between 3.6 and ~0.8 Ma, and gradually decreased thereafter (Fig. 3 *A* and *B*). In line with the rock magnetic and DRS analyses, geochemical analysis shows that the total Fe^{2+} and Fe contents of the TB dust <5 μm fractions have increased significantly over the past ~0.8 Ma (Fig. 3 *C* and *D*).

Quantitative measurements of the structural Fe^{2+} in the <5 μm fraction of the TB dust were performed using hydrofluoric and sulfuric acid digestion with 1,10-phenanthroline as the colorimetric reagent, following conventional procedures (36–40).
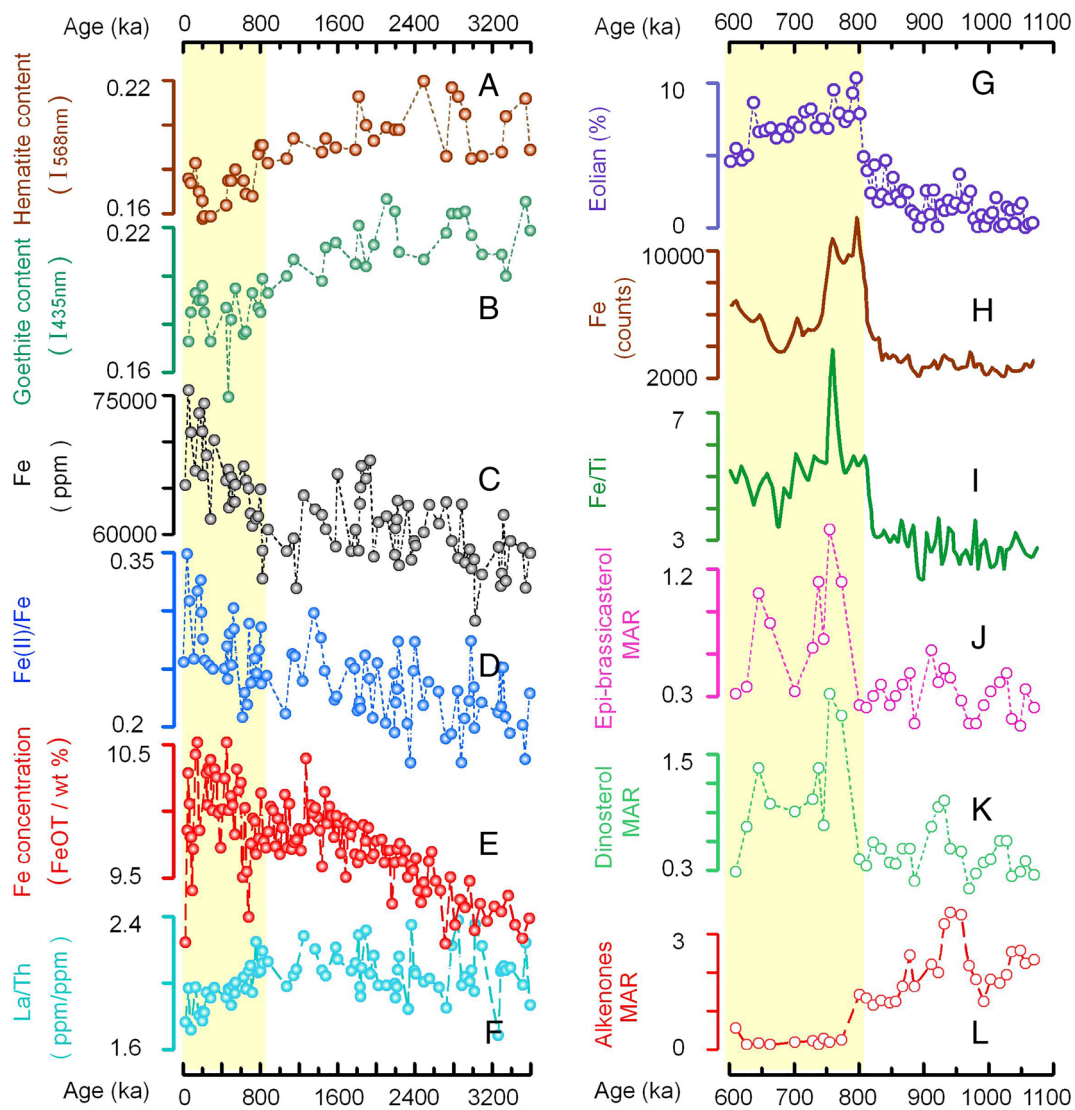
Fig. 3. (*A–D*) Temporal variations in concentrations of hematite, goethite, total Fe and Fe^{2+}/Fe for the <5 μm fraction of the TB dust. (*E*) Total Fe concentration of the <5 μm fraction of eolian dust in the Baishui section, western CLP (35). (*F*) La/Th ratios for the <5 μm fraction of the TB dust. (*G–L*) Eolian weight percentages, Fe counts, Fe/Ti ratio, and the mass accumulation rate (MAR, μg/cm²/kyr) of lipid biomarkers in core PC 932 from the equatorial Pacific (16). Note that total Fe and Fe^{2+} contents of the <5 μm fraction of the dust deposits from the TB, CLP and the equatorial Pacific increased significantly since the mid-Pleistocene. Increased eolian supply of bioavailable Fe after ~0.8 Ma coincides with a dramatic change in the dominant phytoplankton group from alkenones (coccolithophores) to epibrassicasterol (diatoms) and dinosterol (dinoflagellates) in the equatorial Pacific, i.e., from calcifying organisms to siliceous organisms.

Chlorite is a common Fe^{2+}-bearing silicate in Chinese eolian dust deposits. A concurrent increase in the concentrations of chlorite and Fe^{2+}/Fe ratio was observed after 0.8 Ma (Fig. 3*D* and *SI Appendix*, Figs. S3 and S4), indicating that Fe^{2+}-bearing silicate minerals (including chlorite)—together with the increased magnetite content—likely account for the mid-Pleistocene increase in total Fe^{2+} and Fe contents of the TB dust. The Fe^{2+}/Fe_{total} ratios of the TB dust <5 μm fractions increase from 0.2 - 0.25 to 0.25 - 0.35 after the MPT (Fig. 3*D*); values consistent with those obtained for North Pacific sediments (ODP Core 1208) via X-ray absorption spectroscopy (11), indicating the reliability of our geochemical results.

Together, these magnetic, DRS, mineralogical, and geochemical data all indicate that a major shift in the Fe content and speciation of the Asian TB dust occurred around the MPT; the content of stable, highly oxidized hematite in the dust decreased, while the magnetite, Fe^{2+}, and total Fe concentrations all increased significantly. The increasing concentrations of primary, detrital magnetite are responsible for the observed changes in the magnetic properties of the TB dust around the MPT.

Debate exists regarding the relative impacts of increased glacial activities and intensive tectonic deformation, respectively, in producing immense volumes of fresh, unweathered Tibetan detritus (22–24). That the switch in the Asian dust mineralogy was linked with climate state and expansion of Tibetan glacial activity (*SI Appendix, Supplementary Text* and Fig. S5), rather than tectonic events, is indicated by the continuous deposition and subsequent preservation of an extremely thick (671 m) sequence of loess in the TB. Notable also is that higher values of our ferrimagnetic concentration-dependent parameters of χ and IRM_{1T} typically occurred in the glacial-stage TB deposits, especially after the onset of northern Hemisphere glaciations at ~2.7 Ma (*SI Appendix*, Fig. S6). Further, the comparison of our TB χ record with those of the downwind central North Pacific sediments reveals after ~0.8 Ma a common shift of their dominant periodicity from 400-ka to ~100-ka (*SI Appendix*, Fig. S7).

Discussion

The TB dust source changes most sharply in the majority of its compositional characteristics at ~0.8 Ma (Figs. 2 *A–E* and 3 *A–C*

and *F*). Fe concentration (Fig. 3*D*) shows a more gradual, long-term increase between ~2.4 Ma and 0.8 Ma, probably reflecting the onset of enhanced cooling, northern hemisphere glaciations and intensified dust transport, before increasing again sharply at 0.8 Ma. We can compare our unique TB dust record with the iron mineralogy reported for the downwind, terrestrial sediments of the famous CLP (35, 41–43) and for several long, late Pliocene-Pleistocene pelagic sediment cores from the central North Pacific (31, 33), where volcanic eolian supply is essentially constant (~10% of the lithogenic fraction) and TB eolian dust forms the dominant component of the sediment silicate fraction.

Geochemical and neodymium isotopic studies show that dust sourced from the Taklimakan Desert provides a dominant contribution to the lithogenic component of pelagic sediments in the N. Pacific (4, 26). Thus, it can be expected that the MPT switch in the composition of the TB Fe-bearing minerals would be observed synchronously in pelagic-clay sediments from the central North Pacific (Fig. 1).

From basal ages of between ~3.6 and 2.5 Ma, central North Pacific sediment cores NGC55, NGC56 and NP18 all exhibit a long-term decreasing trend in the magnetic concentration-dependent parameters of χ and $IRM_{2.5T}$, until ~0.8 Ma when they reached minimum values (Fig. 2 *G–M*). There is little evidence of diagenetic dissolution of magnetic minerals in these sediments; magnetic grain size, for example, displays no obvious changes, and sub-micrometer magnetite particles formed by magnetotactic bacteria are observed to persist relatively unaltered throughout this time interval (31). Rather, this decline in sediment ferrimagnetic concentration most likely reflects increased fluxes of highly-oxidized, weakly magnetic, hematite-dominated Asian dust (Fig. 2 *N–Q*). The increasing flux of weathered/oxidized Fe^{3+}-rich dust through the interval 3 Ma to 0.8 Ma makes no/little difference to ocean productivity because it is relatively unreactive and unavailable to the ocean fauna.

Thereafter, however, this trend was strongly reversed; sediment ferrimagnetic content increased, and subsequently remained high and variable, while the high-coercivity (hematite-like) component decreased (*SI Appendix*, Fig. S8). This correlation between the TB and pelagic North Pacific records (Fig. 2 and *SI Appendix*, Fig. S7), with their synchronous switch from a hematite- to a magnetite-dominated composition from the MPT onwards, strongly indicates that the composition and concentration of Fe oxides in the central North Pacific sediments changed significantly in response to the mid-Pleistocene shift in the magnetic and Fe mineralogy of the Asian dust (see *SI Appendix* for further discussion of the magnetic properties of the pelagic N. Pacific records).

Similar changes in Fe concentration and speciation are observed in eolian dust deposits from the CLP. After ~0.8 Ma, pronounced increases in total Fe content and the lithogenic magnetic susceptibility of the <5 μm fraction are evident in the CLP loess deposits (Fig. 3*E* and *SI Appendix*, Fig. S9), indicating increasing concentrations of fresh Fe-bearing silicate particles and detrital magnetite, respectively.

Based on this step change in the Fe mineralogy of the Asian dust, recorded synchronously in both the terrestrial realm and the pelagic Pacific sediments, we calculate that the flux of potentially bioavailable Fe^{2+} to the N. Pacific was more than doubled after the MPT; with substantive ramifications for influencing productivity and/or phytoplankton communities via changes in the Fe-fertilized biological pump. Our geochemical analyses of the TB <5 μm dust fractions show that after ~0.8 Ma the average concentration of Fe^{2+} increased by ~40 to 50%, and the average total Fe content of the TB dust increased by ~15% (Fig. 3 *C* and *D*). Synchronously, eolian dust fluxes in the central N. Pacific

increased by ~30 to 50% (Fig. 2 *N* and *O*), likely reflecting enhanced Asian dust delivery due to global cooling and intensified atmospheric circulation (33, 44). Hence, the eolian flux of Fe and Fe^{2+} in Asian dust to the central N. Pacific increased around the MPT by ~70% and ~120%, respectively. Such a large shift in the potential bioavailability of the Asian eolian Fe is likely to have stimulated changes in N. Pacific phytoplankton communities and/or productivity.

Hence, our findings can not only account for the reported decoupling of dust and ocean productivity in the pre-MPT interval; i.e., when Pacific productivity remained low in early Pleistocene glaciations, despite increased dust fluxes. They also indicate that (glaciogenic) changes in Asian dust source genesis, weathering history, and composition were more significant for Fe fertilization and ocean productivity than changes in dust fluxes alone. The increased bioavailability of Fe^{2+}-bearing materials in Asian dust, resulting from the late Cenozoic expansion of mountain glaciers in the N. Tibetan Plateau (*SI Appendix*, Fig. S5), likely strengthened the dust-CO_2-climate feedback loop (1) in the North Pacific region. Sediment proxy records of productivity should thus be considered not just in terms of changing (increasing) fluxes of Asian dust but, critically, from pre- to post-MPT, in terms of its composition and resultant bioavailability.

Notable is the coincidence between the shift in Asian dust bioavailability around the MPT and reported changes in the composition and/or productivity of phytoplankton communities across the North Pacific region.

Recent laboratory culture experiments demonstrate that diatoms can access particulate Fe^{2+} in silicate minerals of eolian dusts without relying on exogenous mobilization of the Fe (45, 46). These findings suggest that particulate Fe^{2+} content in eolian dusts, rather than abiotic solubility, may control Fe bioavailability for diatom growth. Hence, the substantial increases in the Asian dust-sourced fluxes of total Fe and Fe^{2+} to the central N. Pacific since the MPT may have promoted changes not just in productivity but in microfaunal communities, and hence in the relative efficiency of the "soft" and "hard" C pumps, with subsequent impacts on CO_2 drawdown from the atmosphere.

For the sub-Arctic and northwestern Pacific, however, relationships between inputs of Fe in Asian dust and biogeochemical cycles may be difficult to discern. Geochemical data (46) indicate that glacier-derived dust may provide the sub-Arctic Pacific with more bioavailable Fe/unit mass than volcanic ash or Asian desert-derived dust. However, given that the fluxes of volcanic detritus can account for ~30% of the total lithogenic sediments in the sub-Arctic N. Pacific (4, 27), volcanic ash may have played an important role in the total Fe bioavailability in this region. Further, additional Fe sources may impact sub-Arctic productivity, including lateral Fe transport via bottom water circulation, and iceberg-rafting. Primary productivity in these areas may thus be influenced by multiple Fe sources, given the proximity to the Izu-Ogasawara-Mariana volcanic arc or oceanic islands (27, 28). Hence, the central and lower latitude N. Pacific may represent optimum areas to elucidate the dynamical links, past and present, between changes in Asian dust composition and supply and oceanic biogeochemical cycles.

For the South China Sea region, Fe and nutrient concentrations in surface water are important limiting factors for primary productivity (14, 15, 47). Based on modern observational studies (47), dust fluxes to the northern South China Sea estimated from satellite data are high (~18 g/m^2/yr) and strong Asian dust events (especially during springtime) are associated with large phytoplankton blooms (e.g., between twofold and fourfold increases in chlorophyll-a). Notable is that eolian dust fluxes to the northern

South China Sea increased during glacial periods from ~1.8 Ma onward yet primary productivity remained relatively low and constant until ~0.7 Ma (*SI Appendix*, Fig. S6). In contrast, after ~0.7 Ma, productivity increased markedly during the higher dust flux-glaciations (*SI Appendix*, Fig. S6). While the influence of upwelling activity/circulation changes cannot be discounted, the shift to strong correlation between eolian dust fluxes and primary productivity (14, 15) roughly coincides with the MPT change in Asian dust Fe composition.

For the lower latitude N. Pacific, most studies of the effects of eolian Fe supply on productivity have been based on opal records (10, 48–51), and revealed no obvious trend in biogenic opal sedimentation. However, opal accumulation records may conceal productivity and export production changes arising from changes in phytoplankton communities. Recent work on N. Pacific core PC 932 (central equatorial Pacific, 5°53′N, 177°26′W, 4136 m water depth) using lipid biomarkers (16) shows that Asian dust Fe supply after ~0.8 Ma was associated with increased productivity by silica-producing phytoplankton and a large decrease by calcifying organisms (i.e., coccolithophores) (Fig. 3 *G–L*). Notably, the biogenic opal record did not reflect this increased diatom productivity, due to radiolarian-sourced opal production prior to the 0.8 Ma uplift in Fe supply. Given the increased flux of glaciogenic, Fe^{2+}-bearing silicates, it is possible that this community shift to diatoms/dinoflagellates may have resulted from Fe-Si co-fertilization (rather than Fe fertilization alone). Such a shift in plankton ecology, from carbonate- to siliceous-producers, may have decreased the export of $CaCO_3$ (hard C) relative to organic (soft) C, resulting in an increase in the seawater carbonate ion content and thus also drawing down atmospheric CO_2 (52). The sensitivity of productivity, and hence climate, to eolian dust is likely to have been prolonged in those ocean areas where the supply of Fe^{2+}-bearing silicate particles overcame limitation not only of Fe but also of Si. Modern studies indicate that silicate concentrations currently limit diatom growth south of 40°N during summer months (53).

These observations combine to indicate that mechanisms for positive feedback between the MPT Fe speciation shift in the Asian dust and biogeochemical cycles varied by location in the Pacific. Whether through increased surface productivity (South China Sea) and/or microfaunal community changes (equatorial Pacific), these biogeochemical processes exert significant impact on the global carbon cycle. Evidence exists for substantial storage of C in the sediments of the glacial N. Pacific after the MPT (54), at least partly related to increased terrigenous and eolian inputs, and enhanced ballasting and carbon burial.

Our findings indicate that the MPT shifts in Fe speciation and content of the Asian dust may have been more significant than flux changes alone in controlling Fe bioavailability and resultant downwind impacts on phytoplankton productivity, communities, soft and hard biological pumps, and hence the oceanic and global carbon cycle (Fig. 4). Our data indicate that Fe fertilization and atmospheric CO_2 drawdown in the N. Pacific will have been optimized, post-MPT, in late glacial stages, when deglaciation exposed freshly weathered surfaces, springtime eolian transport of Fe^{2+}-rich dust was maximized and Pacific sea ice declined in coverage.

Modeling of the feedbacks between dust supply and changes in atmospheric CO_2 induced via Fe fertilization has so far focused on glacial/interglacial sequences and timescales (1, 55). Here, the major shift in the Fe bioavailability of the Asian eolian dust indicates that the response of atmospheric CO_2 to changes in Pacific dust supply was likely different pre- and post-MPT, and occurred in coincidence with the shift from a 41-kyr to a 100-kyr climate system.

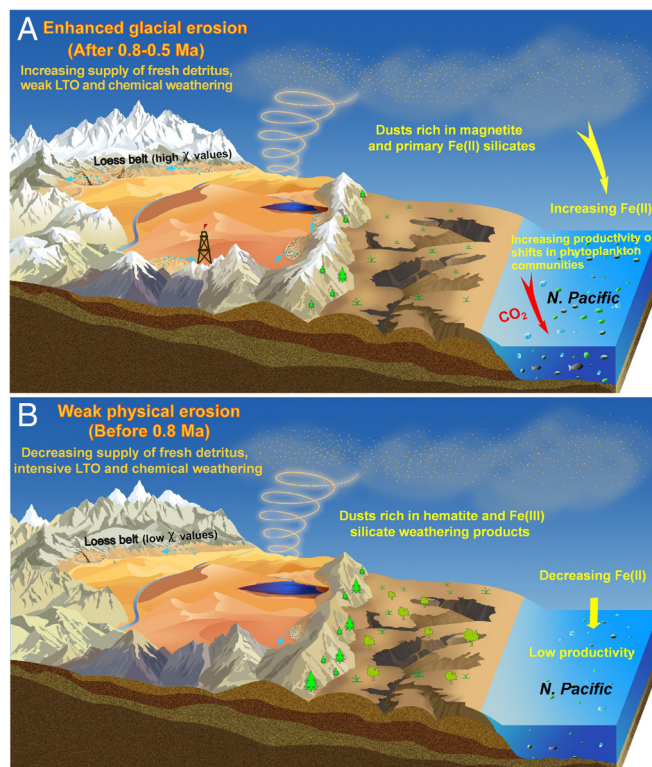It is increasingly evident that productivity and plankton communities in the N. Pacific (and other ocean regions) respond in complex ways to changes in the supply, sources and biogeochemical cycling of Fe and other essential nutrients (56). Across the surface waters of the largest of the world's oceans, Fe and other micro-nutrients can be supplied not only from eolian dust but a diverse range of potential sources (lateral oceanic transport, iceberg rafting, volcanic ash, sedimentary supply) (57, 58). However, the importance of eolian dust for N. Pacific productivity is demonstrated by the direct relationship observed between dust inputs and productivity changes at the present day (12). Uniformitarian principles thus support the likely significance of past changes in Asian eolian dust composition, as well as fluxes, for past changes in N. Pacific productivity and hence in drawdown of atmospheric CO_2.

In summary, our results identify for the first time the major change in Fe speciation and content of Asian eolian dust around the MPT, and hence offer new insights into the dynamic relations between Tibetan glacial erosion and N. Pacific productivity and faunal changes. As a corollary, they point to the possibility that variations in Fe species/concentration of Asian dust records can be used to reconstruct the glacio-erosional history of the N. Tibetan Plateau over geological timescales. Finally, they provide geological context and perspective for the modern-day changes in the bioreactivity of Asian dust caused by release into the atmosphere of anthropogenic Fe-bearing particulate pollution (59).

Methods and Materials

Sampling and Gravitational Separation. The 671-m–deep loess core was obtained from the highest fan surface of the southern margin of the TB, with a recovery of 96.1%. The loess core was firstly cut into two halves for lithologic description and subsampling, and then preserved in cool and dry conditions to

Fig. 4. Conceptual model illustrating the driving mechanism of mid-Pleistocene shift in Fe concentration and speciation of the TB dust, and its possible effects on phytoplankton productivity and community structure in the N. Pacific. Dust particles sourced from the Taklimakan Desert provide a dominant contribution to the lithogenic components of dust deposits both in the TB and the pelagic sediments of the N. Pacific. LTO: low-temperature oxidation.

avoid oxidization or reduction. Bulk loess samples were collected at 20 to 40-cm intervals with a temporal resolution of ~1 to 3 ka. Thereafter, approximately 20 to 30 g of 84 bulk loess samples were prepared for extracting the <5 μm fraction. The <5 μm fraction of the TB loess, which provides the dominant lithogenic materials of Pacific sediments through trans-Pacific dust transport, was separated using Stokes' Law. During gravitational separation, acetic acid rather than hydrochloric acid was used for carbonate removal to avoid significant loss of ferrimagnetic minerals (60). The size-fractionated samples were then collected for further rock magnetic, geochemical, and DRS analyses, with the aim to investigate the temporal variations in Fe speciation and concentration of Asian dust.

Rock Magnetic Analysis . The magnetic susceptibility of bulk and <5 μm fractions of the TB loess was measured using a Bartington Instruments susceptometer at frequencies of 470 and 4,700 Hz. Since the volume of the size-fractionated samples is difficult to obtain, the mass-specific magnetic susceptibility (in units of m^3/kg) rather than volume-specific magnetic susceptibility (SI units) was calculated for the TB loess. In this study, χ values represent low-frequency measurements. The percentage frequency-dependent magnetic susceptibility was defined as: $\chi_{fd}\% = (\chi_{470Hz} - \chi_{4700Hz})/\chi_{470Hz} \times 100\%$. The magnetic susceptibility typically reflects variations in the concentration of ferrimagnetic minerals (maghemite/magnetite) in samples, although it may be affected by other magnetic components when the concentration of ferrimagnetic minerals is low. $\chi_{fd}\%$ primarily reflects variations in the proportional contribution of ultrafine-grained (~0.3 μm) ferrimagnetic minerals, produced by weathering and pedogenesis, to the magnetic susceptibility. The IRM was imparted in a 1 T field using an ASC Pulse Magnetizer, and then measured using a Molspin Minispin magnetometer. IRM reflects the concentration of remanence-bearing material (typically ferrimagnetic maghemite/magnetite and imperfect antiferromagnetic hematite/goethite) to samples.

The temperature-dependent magnetic susceptibility of the <5 μm fraction of the TB dust was measured using a MFK1-FA Kappabridge equipped with a CS-4 high-temperature furnace. The samples were heated from room temperature to 700 °C in an argon atmosphere to minimize any potential oxidation. Low-temperature magnetic measurements of representative samples of the <5 μm fraction were performed using a Quantum Design magnetic property measurement system at the Geomagnetism and Geochronology Laboratory, Institute of Geology and Geophysics, Chinese Academy of Sciences. The low-temperature susceptibility was measured from 20 to 300 K at two frequencies, 1 and 1,000 Hz. The frequency dependence for each temperature (χfd–T) is defined as $\chi fd = \chi 1Hz - \chi 1000Hz$. Ms, irrespective of variations in ferrimagnetic grain size, was determined using a MicroMag 2900 alternating gradient magnetometer.

DRS Analysis. DRS analysis was used to determine semi-quantitatively the contents of hematite and goethite in the TB sediments (61). The size-fractionated samples (<5 μm fractions) of the TB dust were measured using a Purkinje General TU1901 Ultraviolet–visible spectroscopy spectrophotometer with a reflectance sphere from 400 to 700 nm at 1-nm intervals. It is widely accepted that the hematite and goethite are characterized by a unique peak at 568 nm and 435 nm, respectively, in the first-order derivative curve (61). Thus, reflectance data were processed using the first derivative, and the band intensities at 568 nm (I_{568nm}) and 435 nm (I_{435nm}) used as proxies for the relative abundance of hematite and goethite of the TB dust.

Geochemical Analyses. The <5 μm fractions of the TB dust samples were treated with HNO_3 + HF mixture to obtain the total Fe contents. First, ~20 mg of each sample was digested in high-pressure Teflon containers using an HNO_3 + HF mixture. The samples were oven-dried at 190 °C for 24 h. Then HNO_3 was added before heating in the reaction vessel at 150 °C. Finally, the solutions were fixed to

50 mL with ultrapure water. Total Fe concentration and trace element ratios were measured using the Leeman Labs ICP-OES and ICP-MS, respectively. The relative SDs are respectively <2% and <5% for major elements and trace elements.

Fe(II) concentrations of the <5 μm fraction of the TB dust were analyzed by the phenanthroline complexation method following conventional procedures (36, 37). The phenanthroline method provides a convenient and efficient way to determine Fe(II) concentrations in natural sediments (38–40). Thirty milligrams of each sample was dissolved in a polypropylene centrifuge tube by adding 1 mL of 10% 1,10-phenanthroline, 10 mL of 3.6 mol/L H_2SO_4, and 1 mL of 40% hydrofluoric acid. Then the solutions were heated in a water bath at 80°C for 1 h. After all the samples had been digested, 3 mL of the solutions were pipetted to another polypropylene centrifuge tube. Thereafter, 1 mL of 10% 1,10-phenanthroline, 5 mL of ammonium acetate buffer, and 6 mL H_2O were added to the solutions. The mixture was placed in the dark for 20 min to ensure the complete reaction and then analyzed by UV–visible transmission spectroscopy at 510 nm. The reactors used in the analyses were all wrapped in tin foil to avoid the influence of light.

Quantitative Clay Mineral Analysis. Organic matter and carbonates in the clay fractions (<2 μm) of the TB dust were removed through chemical procedures. A total of 50 size-fractionated samples was collected for clay mineral analysis. The oriented smear samples were firstly deposited on glass slides at room temperature, and air-dried aggregates obtained. Subsequently, the smears were treated with ethylene glycol vapor for 24 h and then heated at 450 °C for 2 h. X-ray diffraction patterns of these oriented samples were measured using a Rigaku D/MAX-2000 diffractometer (Cu, Kα, 1.5406 Å, 40 kV, 100 mA, 3 to 30°, step 0.02°, 10°/min). Clay minerals were identified based on the positions of the (001) series of basal reflections (62). Semiquantitative clay mineral results were calculated based on the areas and heights of the diagnostic peaks through Jade 6.5 software (63).

Wavelet Transform and Power Spectrum Analyses. To obtain information about the periodicities of the magnetic parameters of Asian dust over the past 3.6 Ma, wavelet transform and power spectrum analyses were conducted on the χ records of loess deposits from the TB, and pelagic sediments from the central N. Pacific. The wavelet power spectrum analysis was performed based on program provided by Torrence and Compo (64), and the power spectrum analysis was conducted using the REDFIT program provided by Schulz and Mudelsee (65).

Data, Materials, and Software Availability. All data generated and used during this study are included in the *SI Appendix* files.

Author affiliations: ᵃState Key Laboratory of Tibetan Plateau Earth System and Resources Environment, Institute of Tibetan Plateau Research, Chinese Academy of Sciences, Beijing 100101 China; ᵇCollege of Resources and Environment, University of Chinese Academy of Sciences, Beijing 1000449 China; ᶜCentre for Environmental Magnetism & Palaeomagnetism, Lancaster Environment Centre, University of Lancaster, Lancaster LA1 4YQ, UK; ᵈAtmosphere and Ocean Research Institute, The University of Tokyo, Kashiwa 277-8564, Japan; and ᵉSchool of Resource and Environmental Sciences, Linyi University, 276000 Linyi, China

1. A. J. Ridgwell, Implications of the glacial CO₂ "iron hypothesis" for Quaternary climate change. *Geochem. Geophys. Geosyst.* **4**, 1076 (2003).
2. B. A. Maher *et al.*, Global connections between eolian dust, climate and ocean biogeochemistry at the present day and at the last glacial maximum. *Earth Sci. Rev.* **99**, 61–97 (2010).
3. F. Lambert *et al.*, Regional patterns and temporal evolution of ocean iron fertilization and CO₂ drawdown during the last glacial termination. *Earth Planet. Sci. Lett.* **554**, 116675 (2021).
4. T. Pettke, A. N. Halliday, C. M. Hall, D. K. Rea, Dust production and deposition in Asia and the north Pacific Ocean over the past 12 Myr. *Earth Planet. Sci. Lett.* **178**, 397–413 (2000).
5. J. Chen *et al.*, Nd and Sr isotopic characteristics of Chinese deserts: Implications for the provenances of Asian dust. *Geochim. Cosmochim. Ac.* **71**, 3904–3914 (2007).

6. J. P. Huang *et al.*, Long-range transport and vertical structure of Asian dust from CALIPSO and surface measurements during PACDEX. *J. Geophys. Res.* **113**, D23212 (2008).
7. I. Uno *et al.*, Asian dust transported one full circuit around the globe. *Nat. Geosci.* **2**, 557–560 (2009).
8. J. H. Martin, Glacial-interglacial CO₂ change: The iron hypothesis. *Paleoceanography* **5**, 1–13 (1990).
9. T. D. Jickells *et al.*, Global iron connections between desert dust, ocean biogeochemistry and climate. *Science* **308**, 67–71 (2005).
10. G. Winckler, R. F. Anderson, S. L. Jaccard, F. Marcantonio, Ocean dynamics, not dust, have controlled equatorial Pacific productivity over the past 500,000 years. *Proc. Natl. Acad. Sci. U.S.A.* **113**, 6119–6124 (2016).

11. E. M. Shoenfelt, G. Winckler, A. L. Annett, K. R. Hendry, B. C. Bostick, Physical weathering intensity controls bioavailable primary iron (II) silicate content in major global dust sources. *Geophys. Res. Lett.* **46**, 10854–10864 (2019).

12. J. E. Yoon *et al.*, Spatial and temporal variabilities of spring Asian dust events and their impacts on chlorophyll-a concentrations in the western North Pacific Ocean. *Geophys. Res. Lett.* **44**, 1474–1482 (2017).

13. G. H. Haug, D. M. Sigman, R. Tiedemann, T. F. Pedersen, M. Sarnthein, Onset of permanent stratification in the subarctic Pacific Ocean. *Nature* **401**, 779–782 (1999).

14. R. Wang *et al.*, Quaternary biogenic opal records in the South China Sea: Linkages to East Asian monsoon, global ice volume and orbital forcing. *Sci. China Ser. D Earth Sci.* **50**, 710–724 (2007).

15. S. C. Clemens, W. L. Prell, Y. Sun, Z. Liu, G. Chen, Southern hemisphere forcing of Pliocene $\delta^{18}O$ and the evolution of Indo-Asian monsoons. *Paleoceanography* **23**, PA4210 (2008).

16. A. O. Badejo, I. Seo, W. Kim, K. Hyeong, S. J. Ju, Effect of eolian Fe-supply change on the phytoplankton productivity and community in central equatorial Pacific Ocean during the Pleistocene: A lipid biomarker approach. *Org. Geochem.* **112**, 170–176 (2017).

17. A. R. Baker, M. French, K. L. Linge, Trends in aerosol nutrient solubility along a west–east transect of the Saharan dust plume. *Geophys. Res. Lett.* **33**, L07805 (2006).

18. A. W. Schroth, J. Crusius, E. R. Sholkovitz, B. C. Bostick, Iron solubility driven by speciation in dust sources to the ocean. *Nat. Geosci.* **2**, 337–340 (2009).

19. M. P. Bhatia *et al.*, Greenland meltwater as a significant and potentially bioavailable source of iron to the ocean. *Nat. Geosci.* **6**, 274–278 (2013).

20. J. R. Hawkings *et al.*, Ice sheets as a significant source of highly reactive nanoparticulate iron to the oceans. *Nat. Commun.* **5**, 3929 (2014).

21. N. M. Mahowald *et al.*, Aerosol trace metal leaching and impacts on marine microorganisms. *Nat. Commun.* **9**, 2614 (2018).

22. M. E. Raymo, W. F. Ruddiman, Tectonic forcing of late Cenozoic climate. *Nature* **359**, 117–122 (1992).

23. P. Z. Zhang, P. Molnar, W. Downs, Increased sedimentation rates and grain sizes 2–4 Myr ago due to the influence of climate change on erosion rates. *Nature* **410**, 891–897 (2001).

24. F. Herman *et al.*, Worldwide acceleration of mountain erosion under a cooling climate. *Nature* **504**, 423–426 (2013).

25. X. Fang *et al.*, The 3.6-Ma aridity and westerlies history over midlatitude Asia linked with global climatic cooling. *Proc. Natl. Acad. Sci. U.S.A.* **117**, 24729–24734 (2020).

26. C. E. Jones, A. N. Halliday, D. K. Rea, R. M. Owen, Neodymium isotopic variations in North Pacific modern silicate sediment and the insignificance of detrital REE contributions to seawater. *Earth Planet. Sci. Lett.* **127**, 55–66 (1994).

27. I. Bailey *et al.*, Iron fertilisation and biogeochemical cycles in the sub-Arctic northwest Pacific during the late Pliocene intensification of northern hemisphere glaciation. *Earth Planet. Sci. Lett.* **307**, 253–265 (2011).

28. Q. Zhang, Q. Liu, J. Li, Y. Sun, An integrated study of the eolian dust in pelagic sediments from the North Pacific Ocean based on environmental magnetism, transmission electron microscopy, and diffuse reflectance spectroscopy. *J. Geophys. Res.* **123**, 3358–3376 (2018).

29. R. Thompson, F. Oldfield, *Environmental Magnetism* (Allen and Unwin, Winchester, Mass, 1986).

30. B. A. Maher, R. Thompson, *Quaternary Climates, Environments and Magnetism* (Cambridge University Press, Cambridge, 1999).

31. T. Yamazaki, N. Ioka, Environmental rock-magnetism of pelagic clay: Implications for Asian eolian input to the North Pacific since the Pliocene. *Paleoceanography* **12**, 111–124 (1997).

32. Z. Jiang *et al.*, The magnetic and color reflectance properties of hematite: From Earth to Mars. *Rev. Geophys.* **60**, e2020RG000698 (2022).

33. Y. Asahara, $^{87}Sr/^{86}Sr$ variation in north pacific sediments: A record of the Milankovitch cycle in the past 3 million years. *Earth Planet. Sci. Lett.* **171**, 453–464 (1999).

34. J. Y. Shin, K. Hyeong, W. Kim, A sediment magnetic record in the North Pacific across the mid-Pleistocene Transition and its implication on Asian dust evolution. *Front. Earth Sci.* **9**, 789584 (2021).

35. S. Xiong, Z. Ding, Y. Zhu, R. Zhou, H. Lu, A 6 Ma chemical weathering history, the grain size dependence of chemical weathering intensity, and its implications for provenance change of the Chinese loess–red clay deposit. *Quat. Sci. Rev.* **29**, 1911–1922 (2010).

36. J. W. Stucki, The quantitative assay of minerals for Fe^{2+} and Fe^{3+} using 1,10-Phenanthroline: II. A photochemical method. *Soil Sci. Soc. Am. J.* **45**, 633–637 (1981).

37. P. Komadel, Quantitative assay of minerals for Fe^{2+} and Fe^{3+} Using 1,10-Phenanthroline: III. A rapid photochemical method. *Clay Clay miner.* **36**, 379–381 (1988).

38. T. T. Xie *et al.*, Soluble Fe release from iron-bearing clay mineral particles in acid environment and their oxidative potential. *Sci. Total Environ.* **726**, 138650 (2020).

39. J. Jung *et al.*, A microbial driver of clay mineral weathering and bioavailable Fe source under low-temperature conditions. *Front. Microbiol.* **13**, 980078 (2022).

40. D. M. Cwiertny *et al.*, Characterization and acid-mobilization study of iron-containing mineral dust source materials. *J. Geophys. Res.* **113**, D05202 (2008).

41. C. Deng *et al.*, Mineral magnetic variation of the Jiaodao Chinese loess/paleosol sequence and its bearing on long-term climatic variability. *J. Geophys. Res.* **110**, B03103 (2005).

42. X. Y. Lei, L. P. Yue, J. Q. Wang, L. Zhang, Magnetic characteristics and their paleoclimatic significance of Fengzhou loess in the Qinling Mountains of China. *Chin. Sci. Bull.* **43**, 1571–1575 (1998).

43. J. Zan, X. Fang, X. Li, M. Yan, J. Kang, Long-term variations in the lithogenic susceptibility of Chinese eolian deposits since the late Pliocene. *Geophys. Res. Lett.* **46**, 726–735 (2019).

44. D. K. Rea, H. Snoeckx, L. H. Joseph, Late Cenozoic eolian deposition in the North Pacific: Asian drying, Tibetan uplift, and cooling of the northern hemisphere. *Paleoceanography* **13**, 215–224 (1998).

45. E. M. Shoenfelt *et al.*, High particulate iron(II) content in glacially sourced dusts enhances productivity of a model diatom. *Sci. Adv.* **3**, e1700314 (2017).

46. B. G. Koffman *et al.*, Glacial dust surpasses both volcanic ash and desert dust in its iron fertilization potential. *Global Biogeochem. Cy.* **35**, e2020GB006821 (2021).

47. S. H. Wang *et al.*, Can Asian dust trigger phytoplankton blooms in the oligotrophic northern South China Sea?. *Geophys. Res. Lett.* **39**, L05811 (2012).

48. M. Lyle, Bloom without fertilizer. *Nat. Geosci.* **1**, 576–578 (2008).

49. C. L. Ziegler, R. W. Murray, T. Plank, S. R. Hemming, Sources of Fe to the Equatorial Pacific Ocean from the holocene to miocene. *Earth Planet. Sci. Lett.* **270**, 258–270 (2008).

50. E. Calvo, C. Pelejero, L. D. Pena, I. Cacho, G. A. Logan, Eastern equatorial Pacific and related CO_2 changes since the last glacial period. *Proc. Natl Acad. Sci. U.S.A.* **108**, 5537–5541 (2011).

51. K. M. Costa *et al.*, No iron fertilization in the equatorial Pacific Ocean during the last ice age. *Nature* **519**, 519–522 (2016).

52. K. E. Kohfeld, C. L. Quéré, S. P. Harrison, R. F. Anderson, Role of marine biology in glacial-interglacial CO_2 cycles. *Science* **308**, 74–78 (2005).

53. S. Yasunaka, H. Mitsudera, F. Whitney, S. Nakaoka, Nutrient and dissolved inorganic carbon variability in the North Pacific. *J. Oceanogr.* **77**, 3–16 (2021).

54. L. Korff *et al.*, Cyclic magnetite dissolution in Pleistocene sediments of the abyssal northwest Pacific Ocean: Evidence for glacial oxygen depletion and carbon trapping. *Paleoceanography* **31**, 600–624 (2016).

55. L. Bopp, K. E. Kohfeld, C. L. Quéré, O. Aumont, Dust impact on marine biota and atmospheric CO_2 during glacial periods. *Paleoceanography* **18**, 1046 (2003).

56. C. M. Moore *et al.*, Processes and patterns of oceanic nutrient limitation. *Nat. Geosci.* **6**, 701–710 (2013).

57. A. Tagliabue *et al.*, Surface-water iron supplies in the Southern Ocean sustained by deep winter mixing. *Nat. Geosci.* **7**, 314–320 (2014).

58. A. Tagliabue *et al.*, The integral role of iron in ocean biogeochemistry. *Nature* **543**, 51–59 (2017).

59. W. Li *et al.*, Air pollution–aerosol interactions produce more bioavailable iron for ocean ecosystems. *Sci. Adv.* **3**, e1601749 (2017).

60. Q. Z. Hao, F. Oldfield, J. Bloemendal, Z. T. Guo, Particle size separation and evidence for pedogenesis in samples from the Chinese Loess Plateau spanning the past 22 Ma. *Geology* **36**, 727–730 (2008).

61. W. L. Balsam, B. C. Deaton, Sediment dispersal in the Atlantic Ocean: Evaluation by visible light spectra. *Rev. Aquat. Sci.* **4**, 411–447 (1991).

62. D. M. Moore, R. C. Reynolds, *X-ray Diffraction and the Identification and Analysis of Clay Minerals* (Oxford University Press, New York, ed. 2, 1997).

63. L. Zeng *et al.*, *SY/T 5163–2010. Analysis Method for Clay Minerals and Ordinary Non-clay Minerals in Sedimentary Rocks by the X-ray Diffraction* (Petroleum Industry Publishing House Bejing, 2010).

64. D. C. Torrence, G. P. Compo, A practical guide to wavelet analysis. *Bull. Am. Meteorol. Soc.* **79**, 61–78 (1998).

65. M. Schulz, M. Mudelsee, REDFIT: Estimating red-noise spectra directly from unevenly spaced paleoclimatic time series. *Comput. Geosci.* **28**, 421–426 (2002).